Macromolecular Chemistry and Physics
www.mcp-journal.de

Copper–Calcium Poly(Acrylic Acid) Composite Hydrogels as Studied by Electron Paramagnetic Resonance (EPR) Spectroscopy

Haleh H. Haeri, Vanessa Jerschabek, Arash Sadeghi, and Dariush Hinderberger**

Incorporating metal ions into synthetic polymer hydrogels results in toughening of these hydrogels. Herein, it is demonstrated that addition of small volumes of a 0.1 M aq. solution of Cu^{2+}-salts to poly(acrylic acid)-based hydrogels (physically cross-linked by Ca^{2+}) increases their mechanical/rheological properties by several order of magnitude. Continuous wave (CW) and pulsed electron paramagnetic resonance (EPR) spectroscopic techniques reveal that the origin of the observed boost in mechanical properties is due to parts of the hydrogel network that interact with and through hydrated copper ions. With EPR spectroscopy, it is found that these complexes mainly have a sixfold (octahedral) H_2O-coordination shell. Hence, in copper-containing hydrogels, in addition to direct ionic and dipolar (H-bonding) interactions between calcium and carboxylic anions of the side chains of polymer, a second interaction arises from the noncovalent, likely electrostatic interactions of the copper hexaaqua complex and PAA carboxylic acids that are screened through the lower charge density in the hydrated complexes. Also, short-ranged hydrogen-bonded networks of Cu^{2+} with aqueous solvent molecules inside the water-filled regions of the polymeric hydrogel may play a pivotal role. The synergy of these interactions explains the improved elastic properties of copper containing hydrogels.

1. Introduction

Hydrogels are 3D networks of hydrophilic polymers, polyelectrolytes, proteins or small molecules like surfactants. They contain water in large amounts, i.e., they have a high swelling ratio of water to dried gel in percentage of volume or weight (often ten or higher). They can be modified in various ways to respond to environmental stimuli like temperature, pH, charge gradients or magnetic fields and are therefore often counted into the realm of smart soft matter.[1] In the early 1960s, Wichterle and Lim prepared functional prototypes of hydrogels in the form of contact lenses.[2] Their achievement is now considered as the first biomedical application of hydrogels. However, it was soon understood that hydrogels could have a much wider range of applications due to their highly porous microstructure, tunable mechanical properties and high surface area. Therefore, they could potentially have diverse applications in drug delivery, tissue engineering, energy storage, electronics, and biosensing.[3–5]

Structural characterization of hydrogels is often achieved by imaging techniques likes scanning and transmission electron microscopy (SEM and TEM) and atomic force microscopy (AFM). Using these powerful methods, one can obtain information on the nature of the hydrogel, its porosity, surface morphology, and mechanical properties. However, there are some drawbacks to these methods. For example, during SEM measurements, the electron beam could destroy the samples. In electron microscopy, only cryo-TEM can be used to study hydrogels in the swollen state.[6–8]

Hydrogels can also be found in the form of hybrid (composites) organic/polymeric–inorganic materials, which opens new pathways for the design of new smart materials through variation and tuning of the individual components. Among these composite hydrogels, metal-containing hydrogels are an interesting class of materials. On a macroscopic scale, metal-containing hydrogels combine the flexibility and solubility of organic polymers with properties particular to metals like redox, catalytic and magnetic activity. On the molecular scale, metal ions can interact with the polymeric/organic components through complexation and mainly through electrostatic interactions, providing new interaction patterns inside hydrogels leading to specific properties.[9]

In the search of new, environmentally friendly and sustainable materials, Sun et al.[10] proposed poly acrylic acid (PAA) hydrogels, cross-linked by calcium cations. Using calcium minerals even in low concentrations improved the mechanical properties considerably ($G' \approx 10^5$ Pa). In another experiment by the same group, successful hydrogel formation took place in the presence of earth alkaline metal ions and some of the

Dr. H. H. Haeri, V. Jerschabek, A. Sadeghi, Prof. D. Hinderberger
Institut für Chemie
Martin-Luther-Universität Halle-Wittenberg
Von-Danckelmann-Platz 4, Halle (Saale) 06120, Germany
E-mail: haleh.hashemi-haeri@chemie.uni-halle.de;
dariush.hinderberger@chemie.uni-halle.de

The ORCID identification number(s) for the author(s) of this article can be found under https://doi.org/10.1002/macp.202000262.

DOI: 10.1002/macp.202000262

transition metals was reported.[11] However, formation of a hydrogel cross-linked by copper salts was not possible, which is somewhat surprising, as calcium and copper cations can easily replace each other in alginate or hyaluronate-based hydrogels. However, the formed copper-based hydrogels were not as robust as the ones which were cross-linked by calcium cations.[12] On the contrary, chitosan-based hydrogels cross-linked by calcium show a strong affinity for copper cations, which results in structural transitions into a multilayer form.[13] Although these two cations have rather similar physical properties, there are also differences on the atomic level. For example, Ca^{2+} has a larger ionic radius (0.097 nm vs 0.072 nm for Cu^{2+}) and it can bind up to eight ligands in its coordination shell.[14]

This manuscript is motivated by our initial finding that the addition of a small amount of a Cu^{2+}-salt (5% v/v of a 0.1 M solution) to a PAA based hydrogel (cross-linked by Ca^{2+}) leads to a significant strengthening of the mechanical properties of the hydrogel. Inspired by these results and knowing that copper cations behave differently in different gel formation mechanisms, we used electron paramagnetic resonance (EPR) spectroscopy in both continuous wave (CW) and pulsed modes to obtain structural information on the microscopic and nanoscopic level.

EPR is a non-destructive magnetic resonance method and monitors the electronic and geometric structures of paramagnetic centers (like free radicals, paramagnetic metal ions or materials with unpaired electrons). Additionally, it can probe the local environment around these paramagnetic substances. Some materials, such as transition metal ions, intrinsically possess free electrons, while in other materials they have to be introduced artificially to the system of interest by spin probing or spin labeling techniques. These types of probing and labeling using organic nitroxide radicals have been used extensively in the past decades and in different fields of biological and material applications.[15–19]

In the next step, the experimentally obtained EPR results are interpreted using the so called spin Hamiltonian (SH), each of its terms being representative of one of the possible interactions of electron (or nuclear in case of NMR) spins in the presence of a homogeneous magnetic field. Solving the SH using quantum mechanics-based formalisms provides us with a precise picture of the spin system's behavior. In the absence of nuclear spin- and exchange interactions, the SH is governed by the field-dependent electron Zeeman term (EZ) and hyperfine coupling term (HF). For nuclei with spins >1/2, another term is added to the SH; the nuclear quadruple coupling (Q). The subsequent spin Hamiltonian system is then defined as in Equation (1)[15]

$$H_{\text{spin}} = H_{\text{EZ}} + H_{\text{HF}} + H_{\text{Q}} = \beta_{\text{e}}\, B\boldsymbol{g}S + S\boldsymbol{A}I + I\boldsymbol{P}I \quad (1)$$

The EZ (represented by the g-tensor) interactions supply the details of the electronic ground state, oxidation state, spin states (high or low) and local symmetry of the involved metal centers. The hyperfine Hamiltonian term (introduced through the A-tensor) monitors the electron spin interaction with the surrounding nuclear spins and contains two terms; an isotropic term, which is the trace of the principal elements of the A-tensor, and an anisotropic (dipolar) term, which provides information regarding the distance and relative orientation between electron spin and interacting nuclei. The third term, H_{Q}represents the nuclear electric quadrupole interactions and is a measure of the asymmetry of electric charge distribution (which is generated by electrons) and hence, the possible orientations of nearby nuclei (for more details see Section 2.3).

Cu^{2+} as a transition metal ion has one unpaired electron and its local environment can be probed by EPR. Here, we perform CW and pulse EPR spectroscopy on a series of samples with different densities (ratios) of calcium and copper ions. We analyze the consequences that varying copper and calcium ion contents has on the formation, the nanostructure and the mechanical properties of hydrogel. We furthermore study the roles of the used solvent and added bases on hydrogel formation. The mechanical properties of the hydrogels are obtained through rheological measurements.

Finally, we are able to correlate the microscopic/nanoscopic views gained through EPR spectroscopy with the macroscopic data obtained from rheology to obtain new insights into formation, stability and nanostructure of these composite hydrogels.

2. Experimental Section

Poly acrylic acid (M_{w} ≈100 000, 35 wt% in H_2O), ^{13}C-sodium carbonate (99% atom ^{13}C), D_2O (99.96% atom D), $CuSO_4 \cdot 5H_2O$, were purchased from Sigma-Aldrich. Anhydrous granular calcium chloride (6–14 mm, purity specified as ≈90%), and anhydrous $CuCl_2$, powder, ≥99.995% were supplied by Merck (Darmstadt, Germany). Carbonate sodium (Na_2CO_3 anhydrous ≥99.8%) and NaOH (≥99%) were bought from Carl-Roth (Karlsruhe, Germany). Ultrapure water (Milipore Milli-Q) was used for sample preparations.

2.1. Sample Preparation

A reference hydrogel was prepared according to literature.[10] An initial solution of PAA (0.1 M) and $CaCl_2$ (0.1 M) were mixed in equal volume ratios and were stirred together for 30 min. Then, sodium carbonate (0.1 M), in equal volume ratio, was added dropwise to this mixture. The mixture was stirred for another 60 min. The formed hydrogel was removed from the magnetic stirring bar and washed thoroughly with Milli-Q water. Hereafter this hydrogel is referred to as the reference gel (sample 1, for sample numbering cf. **Table 1**) with the general formula PAA:$CaCl_2$:Na_2CO_3, 1:1:1. Subsequently, the prepared sample was stored in vials filled with Milli-Q water and kept at room temperature for later experiments. The pH of the gel-containing solution was found to be basic (pH ≈8–9).

A PAA concentration of 0.01 M was found as the lowest possible concentration to obtain the hydrogels. All composite samples were prepared based on variations of reference hydrogel (sample 1). For the composite hydrogels, $CuCl_2$ (0.1 M) or $CuSO_4$ (0.1 M) stock solutions were used as starting points.

A list of samples which resulted in formation of hydrogels and are discussed in this report, are given in Table 1. Throughout the paper these sample numbers are referred to.

To prepare copper-containing hydrogels, sodium carbonate or calcium chloride was partially substituted, by a 5% or 50% vol of copper chloride or copper sulfate solution. The final volume of the mixture was 15 mL, corresponding to final copper concentrations of 1.6 and 16 × 10^{-3} M, respectively. Hereafter,

Table 1. List of discussed hydrogels characterized by EPR and/or rheometry. The final concentration of calcium and copper content in each sample, are also given.

#Nr.	Sample description (components in vol%)	pH	$[Ca^{2+}]$: $[Cu^{2+}]$ /$\times 10^{-3}$ M
Reference hydrogels (no copper)			
1	PAA:$CaCl_2$:Na_2CO_3 (1:1:1) in Milli-Q water [10]	9.0	33.3: 0.0
2	same ratios as in 1, in deuterium oxide	8.8	"
3	PAA:$CaCl_2$ (1:1) NaOH instead of Na_2CO_3	11.1	"
Copper containing hydrogels (variation of the Cu^{2+}: Na_2CO_3 ratios)			
4	PAA:$CaCl_2$:Na_2CO_3:$CuCl_2$ (1:1:0.95:0.05)	8.0	33.3: 1.6
5	PAA:$CaCl_2$:Na_2CO_3:$CuCl_2$ (1:1:0.5:0.5)	5.1	33.3: 16.6
6	PAA:$CaCl_2$:Na_2CO_3:$CuSO_4$ (1:1:0.95:0.05)	9.1	33.3: 1.6
7	PAA:$CaCl_2$:Na_2CO_3:$CuSO_4$ (1:1:0.5:0.5)	8.2	33.3: 16.6
8	PAA:$CaCl_2$:$CuCl_2$/NaOH (1:1:0.05)	8.6	33.3: 1.6
Copper containing hydrogels (variation of the Cu^{2+}: Ca^{2+} ratios)			
9	PAA:$CaCl_2$:Na_2CO_3:$CuCl_2$ (1:0.9:1:0.1)	8.6	30.0: 3.3
10	PAA:$CaCl_2$:Na_2CO_3:$CuCl_2$ (1:0.5:1:0.5)	8.4	16.6: 16.6
copper containing isotope hydrogels			
11	same ratios as in 4, with 1:1 H_2O:D_2O as solvent	8.0	33.3: 1.6
12	same ratios as in 4, using $Na_2{}^{13}CO_3$	8.0	33.3: 1.6
spin probe (TEMPO) containing hydrogel			
13	PAA:$CaCl_2$:Na_2CO_3:TEMPO (1:1:0.95:0.05)	8.7	33.3: 0.0
14	$CaCl_2$:Na_2CO_3:$CuCl_2$ (1:0.95:0.05)	7.8	33.3: 1.6
sample without PAA			

these samples are referred with their volume percent ratio. Copper salt solutions were added to the mixture in the second step and the new mixture was stirred for another 60 min (samples 4 to 7 in Table 1).

Sample 4 was modified to make two other samples; sample 11 in which a 1:1 mixture of light and heavy water was used as solvent and sample 12 that contains ^{13}C sodium carbonates.

The base was varied and the pH of the solution was adjusted by sodium hydroxide (0.1 M) instead of the originally used sodium carbonate until the hydrogel formation pH reached about ≈8–9 (sample 3). The corresponding composite hydrogel with 5% $CuCl_2$ could also be formed (sample 8).

To test for the effect of variation in the concentration of calcium ions, the relative calcium ion content was decreased to 90 vol% (30×10^{-3} M) and 50 vol% (16.6×10^{-3} M) and was replaced by copper chloride solution (samples 9 and 10). Replacing 100% of calcium salts with the respective copper salts did not result in hydrogel formation, neither in H_2O nor in D_2O, as described previously.[11]

Additionally, to characterize the hydrogel formation and its properties also with an amphiphilic organic spin probe, a nitroxide containing sample was prepared using the nitroxide radical TEMPO (2,2,6,6-Tetramethylpiperidinyloxyl) with a typical final concentration of 200×10^{-6} M (sample 13). It is amply shown that in particular using TEMPO, hydrophobic regions in polymeric or protein samples can be detected even at very small volume fractions.[20–22]

The samples were loaded into 3 mm (outer diameter) EPR quartz tubes (Qsil, Germany), vitrified in pre-cooled 2-methyl butane and frozen in liquid nitrogen. Finally, the samples were stored at –80 °C for further measurements. The same sample was used for CW- and pulsed EPR measurements.

2.2. Rheological/Mechanical Characterization

Rheological characterization of the hydrogels was performed on an Anton Paar Physica MCR 301 (Anton Paar, Graz, Austria) rheometer, using a 25 mm parallel-cone plate geometry. The samples were carefully placed on the surface of the lower plate and the upper plate was lowered to a 0.051 mm gap distance. Frequency sweep measurements were performed in the oscillatory mode with a deformation factor $\gamma = 0.1$ increasing from 0.1 to 100 (1/s) in 16 and 31 steps. Both showed the same trend. Here, the experiments with 31 points are shown.

2.3. CW and Pulsed EPR Spectroscopy and Data Analysis

Q-band CW-EPR (33.9 GHz) measurements were conducted on a Bruker EMX-plusQ spectrometer, using an ER5106QT resonator. A microwave power of 0.1 mW was applied for all samples and for all background measurements. Unless noted otherwise, a modulation amplitude of 0.5 mT was used during measurements. The modulation frequency was set to 100 kHz and measuring temperature was 20 K. A Sumitomo cryo compressor-F70 was used for cooling together with a Mercury iTC (Oxford Instruments) to control the temperature.

X-band (≈9.4 GHz) pulsed EPR measurements were performed on an Elexsys E580 EPR spectrometer equipped with

an MS3-114 resonator (Bruker, Karlsruhe-Germany). The pulses were amplified by a 1 kW pulsed travelling wave tube (TWT) amplifier (Applied system Engineering, Texas, US, Model117). Field swept electron spin echo (ESE)-detected spectra, three-pulse electron spin echo envelope modulation (ESEEM), and hyperfine sublevel correlation spectroscopy (HYSCORE) time domain data were recorded at 20 K. A closed cycle cryostat (ARS- 4WH, www.arscryo.com) was used for cooling during measurements. For all $\frac{\pi}{2}$ microwave pulses a 16 ns pulse length and for π microwave pulses a 32 ns pulse length were applied. The Hahn echo sequence[23] ($\frac{\pi}{2}-\tau-\pi-\tau-\text{echo}$) had an initial inter-pulse delay of $\tau = 176$ ns.

The three-pulse ESEEM ($\frac{\pi}{2}-\tau-\frac{\pi}{2}-T-\frac{\pi}{2}-\tau-\text{echo}$) were used with four step phase cycling to eliminate the unwanted echoes.[24,25] The chosen τ values were 176 ns and the second inter-pulsed delay (T) was set to 300 ns, incremented in 16 ns steps. For samples containing isotope-enriched nuclei (^{2}H, ^{13}C), blind spot behavior of ESEEM and HYSCORE may be different and the following setups were tried as well. In the case of deuterated samples $\tau = 344$ ns combined with $T = 80$ ns incremented in steps of 8 ns was also tried, to minimize the proton modulation influence.[26] For the sample containing ^{13}C, the ESEEM data were collected using τ = 408 ns, T = 386 ns incremented in 12 ns, to suppress the proton modulations and enhance the ^{13}C modulations.[27] As significant difference was not observed in results obtained by $\tau = 176$ ns, the latter data is reported.

Three-pulse ESEEM time traces were processed using a home-written MATLAB (MATLAB R2016a, The MathWorks & Inc., Natick, MA, USA) code. They were first baseline corrected (using a stretched exponential function), apodized with a Hamming window and then zero-filled to 1024 points. Finally, Fourier transformation provided the magnitude spectra.

HYSCORE[28] is a 2D four-pulse ESEEM experiment, which correlates the ESEEM frequencies (nuclear transitions) between two different M_s manifolds. The spectra were collected using the sequence ($\frac{\pi}{2}-\tau-\frac{\pi}{2}-t_1-\pi-t_2-\frac{\pi}{2}-\tau-\text{echo}$), where t_1 and t_2 denote the incremented mixing times. The typical value of 176 ns was chosen for the inter-pulse time τ and the delay times $t_1 = t_2$ were set to 300 ns initially. A time increment of 16 ns (data matrix 256 × 256), together with an eight step phase cycling were used. All HYSCORE data were processed with a home written MATLAB code (MATLAB R2016a, The MathWorks, & Inc., Natick, MA, USA). Polynomials (order 3 or 5) were used for background corrections. Then, they were apodized by a Hamming window and zero filled to 1024 points. A 2D Fourier transformation provided the magnitude spectra. After Fourier transformation, the correlation between two frequencies of the same nuclei, at different spin manifolds (ν_α, ν_β), can be seen as anti-diagonal peaks, similar to correlation spectroscopy in NMR (the so-called cross peaks). These cross peaks appear in the (+, +) and (+, −) quadrants and show the weakly and strongly coupled nuclei to the paramagnetic center at their Larmor frequency, respectively. The shift of cross peaks away from the diagonal gives an initial estimation of the hyperfine of the nucleus ($A \sim \nu_\alpha - \nu_\beta$). Also, the maximum shift value along anti-diagonal ($\Delta\omega_{max}$) provides with the magnitude of the dipolar part of the hyperfine tensor, T, in an axial hyperfine tensor ($-T, -T, 2T$), according to the Equation (2)

$$\Delta\omega_{max} = \frac{9T^2}{32\omega_i} \tag{2}$$

in which, ω_i is the nuclear Larmor frequency of the corresponding i-th nucleus.[15] By simulating the HYSCORE spectra at different field positions, detailed information of the hyperfine tensors was obtained for the system of interest.

The distance between two dipolar coupled nuclei can be extracted using the point dipole approximation,[29,30,31] Equation (3)

$$T = \frac{\mu_0}{4\pi h}\frac{g_e g_n \beta_e \beta_n}{r^3} \tag{3}$$

The principal elements of the traceless quadrupole tensor P, are defined as follows

$$P_z = \frac{e^2 Qq}{2I(2I-1)h}; \eta = \frac{P_x - P_y}{P_z} \tag{4}$$

By definition, Q is the nuclear quadrupole moment, eq is the electric field gradient or electrical shape of the nucleus and η is the asymmetry parameter, which shows the deviation of the field gradient from uniaxial symmetry about Z.[30,31]

All simulations of CW- and pulsed- spectra, were performed using Easyspin program package (version 5.2.27) in MATLAB.[32] Natural isotope abundancies for all nuclei were used throughout the simulations.

2.3.1. EPR Reference measurements

Reference measurements were made under exactly the same conditions as other measurements on the pure PAA solution, salt solutions ($CaCl_2$ and Na_2CO_3 plus 20% vol of glycerol as cryo- protectant (80% wt from Thermo Fisher) and of the prepared reference hydrogel (sample 1). In comparison to other magnetic resonance techniques (like standard NMR spectroscopy), EPR spectroscopy is a very sensitive technique. Even small amounts of the paramagnetic material (in the ppm range) returns an EPR signal. A trace of a paramagnetic substance centered on a 3/2 nuclear spin (I = 3/2) signal was observed in the salts mixture ($CaCl_2$-Na_2CO_3) and therefore in the reference hydrogel, sample 1 (Figure S1, Supporting Information). This signal is clearly visible in both CW- and pulsed-EPR measurements. The double integration of the area under EPR spectrum shows the quantity of this impurity, which is about 13% comparing two samples (1) (reference hydrogel nominally without copper) and (4) (with 5% $CuCl_2$). Since the spectral pattern and the parameters are very similar to those of Cu^{2+}, this impurity is assigned in copper-less reference samples to be Cu^{2+}, stemming from the technical grade (≈90%) granular calcium chloride. Therefore, one should be aware of such naturally occurring copper ions when using technical grade salts in these hydrogels in the future. Potentially, experimental data that were hard to explain could be re-investigated in light of this finding.

3. Results and Discussion

3.1. Rheological Characterization

3.1.1. Reference Hydrogel (Sample 1)

The prepared reference hydrogel (sample 1) possesses large elastic (storage) and viscosity (loss) moduli of ≈10^4–10^5 Pa, and hence high visco-elastic properties (**Figure 1**). The complex viscosity value, η^*, decreases heavily with increasing angular frequency. The same holds true for the here-reported composite hydrogels, confirming they are pseudo-plastic fluids with shear thinning behavior.

3.1.2. $CuCl_2$ Containing Hydrogels (Samples 4 and 5)

Addition of copper salt (≈5%v/v ≈1.6×10^{-3} M) while keeping the calcium salt contents fixed at ≈33×10^{-3} M (sample 4), increases both elasticity and viscosity of the hydrogel to values above 10^6 Pa, potentially due to incorporation of an even larger amount of metal ions[33] in the system. The $G' > G''$ values are also an indication that in this hydrogel the metal ions are strongly associated in the polymer network. Since these values are rather invariant with changing angular frequency, we conclude that the hydrogels are rather well structured (Figure 1).

Increasing the copper ion content to ≈50%v/v (≈16×10^{-3} M, sample 5) improves the mechanical properties as compared to the reference hydrogel (1), as well. The storage and loss moduli still denote a tough hydrogel but their values are slightly lower than the one with 5% copper ion content. From visual/physical inspection, hydrogel (5) is more rubber like. Figure 1 shows the storage and loss modulus of copper ion-containing hydrogels in comparison with the reference hydrogel (1).

When using $CuCl_2$ and varying its relative content from 5% to 50%, we observed a sharp decrease in pH of more than three units (from 8.5 to 5.1). At lower pH, the carboxylic acids of the polyelectrolyte PAA are largely protonated, which is not favored by calcium (as a hard acid, calcium prefers increased deprotonation of PAA based in a simple HSAB view of calcium binding) and therefore a weaker hydrogel is formed. Also at lower pH, there is a competition between protons and copper ions to interact with the carboxylic acid groups of the polymer, which is why more copper ions may be able diffuse in the sample as the hexaaqua complex. This may be the reason for the rich blue color observed in hydrogel 5 (see Figure 1C)).

3.1.3. $CuSO_4$ Containing Hydrogels (Samples 6 and 7)

The mechanical properties of hydrogels prepared with copper sulfate are similar to those of the reference hydrogel (1), although in both cases, the viscosity is slightly more dominant and $G'' > G'$, (Figure 1B). Therefore, apparently the strengthening of the polymer network is not as strong as in case of $CuCl_2$-containing hydrogels. This could be related to the stronger electrostatic repulsion forces between the negatively charged carboxylates of the PAA polymer and divalent sulfate anions and stronger electrostatic attraction of sulfate and copper ions, both when compared to interactions with monovalent chloride anions. The anion size could also play a role,

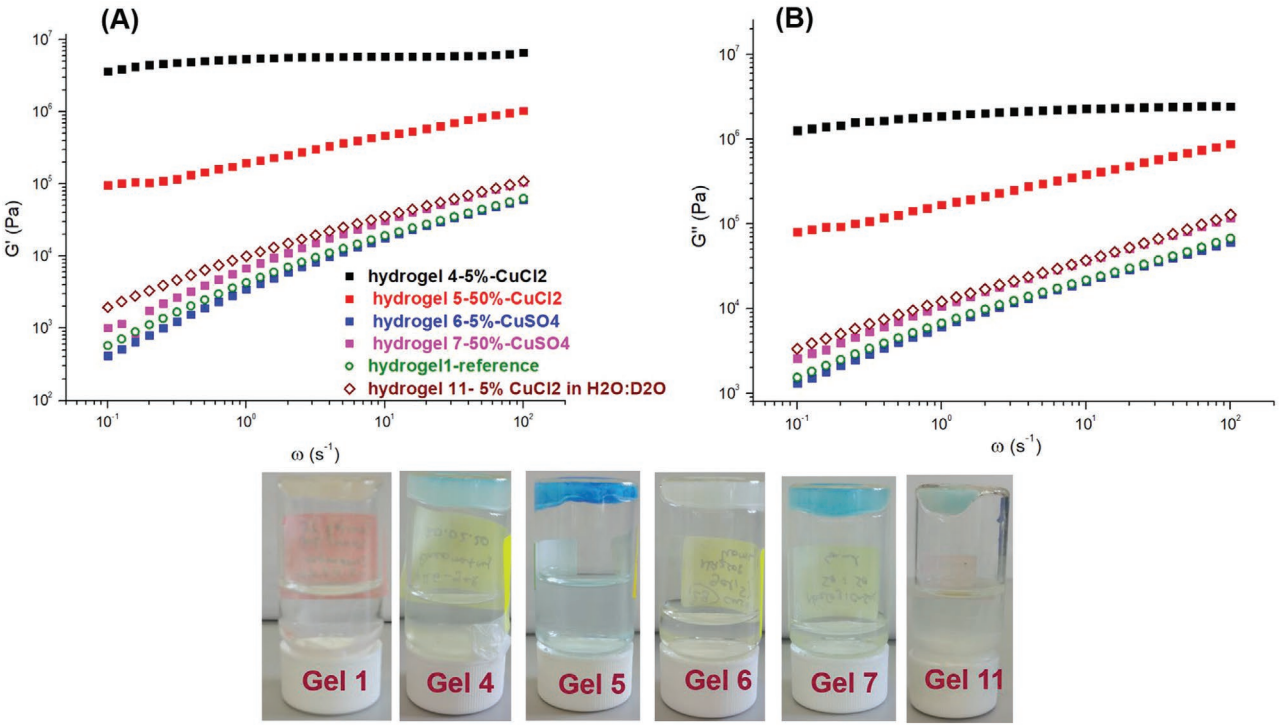

Figure 1. Mechanical properties of the composite hydrogels as measured through A) storage G' and B) loss modulus G''. The sample numbering is according to Table 1. C) The inversion test confirms the physical gel state of all copper containing hydrogels, with their corresponding sample numbers.

as sulfates are bigger and heavier than the chlorides and may co-diffuse with copper ions.

Using higher content of $CuSO_4$ (50% v/v), there was no such pronounced change in pH (from 9.1 to 8.2). This indicates the deprotonation of PAA is not affected by sulfate ions as much as it is by chloride counterions of Cu^{2+}.

3.1.4. Variation in Calcium Salt Content (Hydrogels 9 and 10)

Decreasing the amount of Ca^{2+} to 90% v/v (30×10^{-3} M in total volume of 15 mL) and replacing it by Cu^{2+} (sample 9), we observe an increase in both G' and G'' moduli to $\approx 10^6$ Pa, compared to reference hydrogel (1) (**Figure 2**). Since their values are invariant with angular frequency, hydrogel 9 shows a stable mechanical behavior over time.

When further substituting the calcium ion content by copper ions (50% v/v each, sample 10), we still observe hydrogel formation with only a significantly reduced G'' compared to hydrogel 9. Hydrogel 10 also shows a clear volume shrinkage (see Figure 2, right hand side), which taken together could be an indication of strong but intricate inter- and intra-molecular interactions between the polymer chains with increasing copper ion content. This could, e.g., be a sign of the formation of multi-layered structures.[13] The elastic module (G') stays stable over time but the viscosity module, G'', has a non-linear behavior at lower frequencies (Figure 2).

3.1.5. Change in Basicity Conditions of Hydrogel Formation (Sample 3)

Using sodium hydroxide instead of sodium carbonate to adjust the pH conditions dramatically improves the visco-elastic properties of the hydrogel (>10^6 Pa), especially at the lower frequencies or long-term behavior area. At this point, one may speculate that this could be attributed to the formation of the hydrogen bonds within the hydrogel network, which may be disrupted at high shear rates but persist and strengthen the hydrogel at low frequencies (**Figure 3**). At frequencies larger than ≈4 Hz, the hydrogels prepared with NaOH reach the moduli of the reference hydrogel 1.

3.1.6. Isotope Effect

Rheometry measurements of sample (11) (5% copper containing sample prepared with a 1:1 H_2O:D_2O solvent mixture), reveals much weaker viscoelastic properties of this hydrogel compared to the corresponding conventional H_2O-based sample, (cf. Figure 1). This already indicates the pivotal role of water and the H-bonding system (which is isotope-dependent) in strengthening of the hydrogel network. The molecular origins of this effect are discussed in Section 3.3.

3.2. CW-EPR Measurements

3.2.1. Copper-Calcium Composite Hydrogels

The EPR spectrum of the 5% $CuCl_2$ containing hydrogel 4 yields the typical signature of an anisotropic, axial EPR signal ($g_{II} = 2.352 > g_{\perp} = 2.067 > g_e = 2.0023$) with an unpaired electron mainly centered in the $3d_{x^2-y^2}$ orbital of the copper cation. This spectral signature is observable when the coordination geometries correspond to an elongated octahedron, a square pyramid or a square plane.[34–38] A trace of a 3/2 species (impurity) in the salts, as explained above in Section 2.3.1., is present from the calcium salt of technical grade. In the samples with Cu^{2+} ions, this paramagnetic species can be seen only dimly as a fifth splitting located in the parallel region of the spectrum with a hyperfine coupling that is one third of that of the intentionally

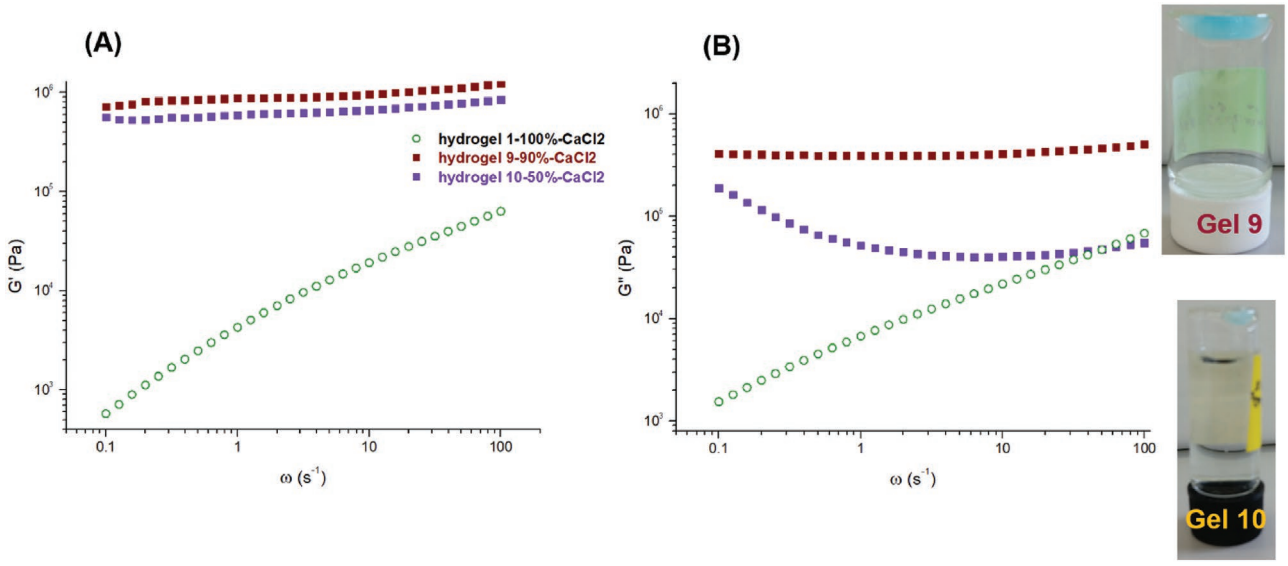

Figure 2. Mechanical properties of copper-containing hydrogels with different calcium content as measured A) through storage G', and B) loss modulus G''. Pictures showing the inversion test and the macroscopic gel-state are shown on the right hand side.

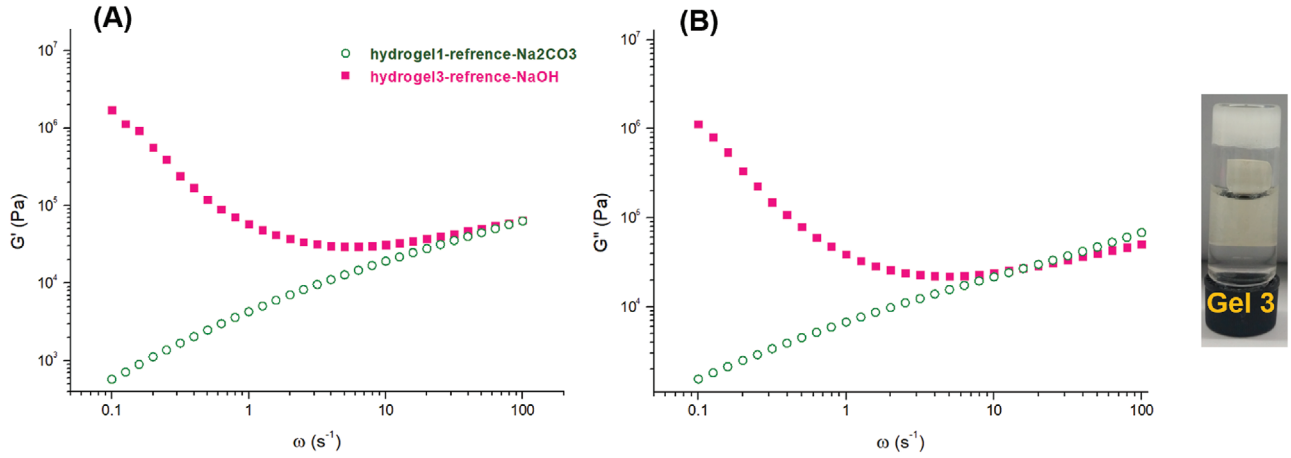

Figure 3. Effect of replacing Na_2CO_3 (hydrogel (1)) with NaOH (hydrogel (3)) to test for the effect of basic conditions on the mechanical properties as measured A) through storage *G′*, and B) loss modulus *G″*. A picture showing the inversion test and the macroscopic gel-state are shown on the right hand side.

added copper ions. The experimental spectrum and its simulation are given in **Figure 4**A).

In the 50% $CuCl_2$-containing hydrogel 5 (Figure 4B), the copper cation concentration is increased tenfold (≈16 × 10^{-3} M) as compared to hydrogel 4. Assuming the superposition of spectra by two different Cu^{2+} species can reproduce the experimental spectrum quite well: the first species with a A_{II} = 490 MHz, could be considered as the main component of the spectrum (contributing ≈70% to the observed spectrum) and is present in most of our prepared samples. Due to the presence of copper complexes with slightly different orientations, g-strain conditions need to be applied to reproduce the experimental spectrum. The second component has a broader line width and higher g-anisotropy, especially at its parallel position. The very broad signal that can be seen in Figure 4B stems from overlapping of these two components. As this solution has a pH of ≈5, the bimodal spectra could be due to co-existence of different copper complexes. The broadness of the signal could be explained by the high local concentration and the local confinement of copper ions in the PAA-based hydrogels, which leads to mainly dipolar (through-space) broadening at low temperatures. Also, in the presence of chloride anions, the pH becomes heavily acidic. Along with decreasing pH, an increase of g_{II} is observed together with the formation of another complex (second species). For most cases we have seen strain effects (especially on g values) arising from slightly differently oriented complexes, however this effect is more pronounced for the high-copper concentration hydrogel 5. The simulation of the EPR spectrum of a 50% $CuCl_2$ containing gel is given in Figure 4B. When using copper sulfate, there are no big differences in the shape or spectral parameters of the prepared hydrogels at the two different ratios and, as stated above, there are only minute differences in their final pH values. The EPR spectral parameters indicate a fully hydrated copper complex at both ratios (Figure S2, Supporting Information).

When comparing experimental spectra in terms of copper/calcium ion content, we observe that when the copper content is fixed at 5%, while calcium salt contents is varied (100%, 90%, and 50%, hydrogels 4, 9, and 10), there are no changes in line width, line shape or intensity of the Cu^{2+} EPR signals. On the other hand, increasing the copper ion ratio from 5% to 50% (hydrogels 4 and 5) the signal intensity increases, which is trivial since the spin content is increased, and the line width (HWHM) enormously increases only for the $CuCl_2$ containing samples (ΔB ≈16 mT). Remarkably, such a broadened line width due to the copper ion content cannot be seen for hydrogels of different $CuSO_4$ contents (samples 6 and 7). The line width remains at ≈11 mT for $CuSO_4$-based hydrogels for both contents (see **Table 2**).

Simulations confirm that the sample 7 (with 50% $CuSO_4$) has the narrowest line width, which at this point might be attributed to be a consequence of the bigger anion size of sulfate compared to chloride (258 vs 167 pm).[39,40] As a result, stronger repulsion between these anions (which attract Cu^{2+} ions) and the negatively charged PAA gel become more important, which leads to a less crowded medium and potentially to a large fraction of copper ions not being embedded in the hydrogel network.

3.2.2. Composite Hydrogels with Different Calcium Contents

In the samples described above, the calcium ion content was always identical. To characterize the effect of calcium concentration (content) on the composite hydrogels, we prepared and tested different samples in which the calcium ions are partially replaced by copper, keeping all other ratios unchanged. The general notation for these hydrogels is PAA:$CaCl_2$:Na_2CO_3:$CuCl_2$ (1:*x*:1:*y*). Samples containing 90% (sample 9 in Table 1) and 50% (sample 10) of calcium were prepared. The EPR spectra of the principal copper components of hydrogels 9 and 10 could be simulated with parameters similar to those obtained for other hydrogels (see Table 2 and Figure S2C,D, Supporting Information), however the EPR spectrum of sample 10 shows a sharp signal at *g* ≈2.001 which is temperature-dependent. While this feature has significant intensity at 20 K, it is strongly diminished at 150 K, which suggests that this is a signature of an inorganic species with a strong temperature dependence in

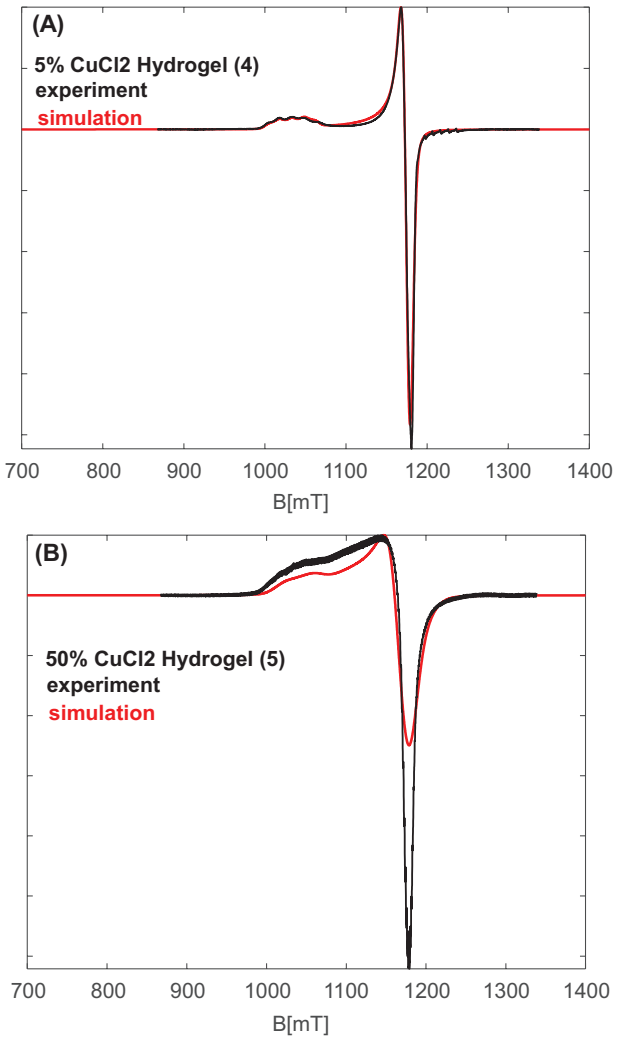

Figure 4. Low temperature Q-band EPR spectra of copper-containing hydrogels. A) Spectrum of hydrogel 4 (5% $CuCl_2$) and its simulation. The five-line splitting in the parallel region is observable due to the overlapping with a second $I = 3/2$ species ($A_{||}$ = 170 MHz from simulations) which stems from technical grade calcium salts and therefore contributes to all prepared samples. B) Spectrum of sample 5 (50% $CuCl_2$) and its simulation. The broadness of the parallel region is attributed to the presence of a second copper complex together with *g*-strain effects. The simulation parameters are given in Table 2.

its T_1-relaxation (**Figure 5**). We performed reference measurements of the empty resonator at different temperatures (using different microwave powers), which did not reveal any signal at this field position. We suppose this signal might be attributed to a metal/polymer (carboxylate)-based species with short lifetime and different relaxation behavior.

Comparing the obtained simulation parameters to the ones obtained for similar cases in zeolites and copper carbonate complexes, reveals that copper is in its fully hydrated complex form, but spectroscopically a minor component of copper complexes rather fits the experimental values of not fully hydrated complexes. As stated above, these values rather resemble those of partially carbonate-/carboxylic acid-ligated complexes in all of the above-mentioned hydrogels. The broadness of the spectra, which is known as a sign of fully hydrated complex,[41–43] could arise as well due to the presence of different conformations with different geometries. The rest of the measured/simulated spectra can be found in Figure S2, Supporting Information.

3.2.3. Nitroxide Containing Hydrogel (Sample 13)

We also tried to study hydrogels using the amphiphilic organic nitroxide radical TEMPO instead of copper ions. This would be possible if there are any direct interactions between the organic spin probe and the polymer chains. TEMPO has an amphiphilic nature (partition factor $P_{OW} \approx 90$), it can monitor both hydrophobic and hydrophilic media and even induce aqueous lower polarity solvation shells in water.[44] We have amply used TEMPO, e.g., to study nanoscopic inhomogeneities in stimuli-responsive polymers.[20–22] By CW-EPR measurements at room temperature and X-band (mw frequency ≈9.4 GHz), we found a strong background signal due to an inorganic impurity, as described in Section 2.3.1., that resembles a copper ion spectrum and that dominates the EPR spectrum at low temperatures (Figure S3, Supporting Information). The TEMPO EPR signal could, however, be well observed at low temperatures (150 K) and at higher resolutions at Q band frequencies (34 GHz). The simulations indicate that the spin probe is located in a hydrophilic medium (A_{zz} ≈1.7 mT), however its motion is severely restricted as evidenced by the very slow isotropic rotational correlation time (≈56 ns). One possible scenario explaining this could be that the spin probe TEMPO is confined in aqueous voids of the hydrogel network, in an environment similar to copper ions and without electrostatic/direct ligand binding to PAA, so that the local viscosity is high but not close to the extremely high macroscopic mechanical stiffness. The experimental and simulated spectra are shown in **Figure 6**.

3.3. Pulsed EPR Measurements

3.3.1. Electron Spin Echo Experiments

Electron spin echoes (ESE) are sensitive to broadening, relaxation rates of the involved paramagnetic nuclei and nuclear modulations[45] and all these factors contribute to the echo shape and intensity.

Despite its low intensity, the signal due to the initial copper in the nominally copper-free reference hydrogel (1) is clearly observable. To test the effect of the polymer PAA of the hydrogel network on the EPR spectra, we prepared a sample composed of sample (1) components but without PAA (denoted as sample14, Table 1). In the usual process of hydrogel formation, addition of the copper salt solution is the last step, which means that the hydrogel network is already formed. We may speculate that in the absence of PAA, copper ions form complexes with available carbonates in the solution mixture and therefore the signal intensity is drastically decreased. In a hydrogel, however, copper ions are probably captured in the interstitial (hollow) regions inside the hydrogel network in a hydrated form and therefore the signal intensity rises again. We discuss the copper cation localization in the hydrogels in detail in the discussion

Table 2. Simulation parameters of the samples with different copper ion and calcium ion ratios.

Nr.[a)]	Comment	($A_\perp$, A_{II}) /MHz	($g_\perp$,g_{II})	Line width /mT
4	5%$CuCl_2$	(50, 490)	(2.067, 2.352)	(8, 4)
5	50%$CuCl_2$ component1 (70%) 50%$CuCl_2$ component 2 (30%) *g*-strain = [0.08 0.07]	(50, 490) (150, 450)	(2.075, 2.225) (2.076, 2.338)	(11, 3) (11, 8)
6	5%$CuSO_4$	(50, 490)	(2.067, 2.352)	(8, 4)
7	50%$CuSO_4$, *g*-strain = [0.001 0.005]	(30, 490)	(2.070, 2.355)	(2.5, 7)
8	5%$CuCl_2$@NaOH	(70, 490)	(2.066, 2.354)	(9, 3)
9	90% $CaCl_2$	(50, 480)	(2.068, 2.352)	(7.5, 4)
10	50% $CaCl_2$	(10, 480)	(2.067, 2.352)	(9, 2)
13	5%TEMPO	(19.5, 15.3, 95.2)	(2.0089 2.0058 2.0025)	(0.3, 0.6)

[a)]For all samples except for #13, the additional copper ion signal with an axial hyperfine tensor [10, 170] MHz is considered. The volume of the composite is given in percent. The Voigtian line widths are given with the Gaussian (first number) and Lorentzian (second number) components.

section. The Cu^{2+}-signal in the reference sample (1) prepared in fully deuterated solvents (sample 2, Table 1) has a very small intensity. The reason for observing such a poor signal is later discussed in the conclusion.

The ESE of the hydrogel with a high content in $CuCl_2$ (sample 5) shows a very broad signal of considerably low signal-to-noise ratio. It is in agreement with what we observed before by CW- EPR experiments, indicating formation of copper complexes with slightly different g-anisotropy and the loss of free copper ions due to the formation of copper-carbonate complexes at the sample's pH of ≈5.0. The high copper content sample containing $CuSO_4$ (sample 7) looks very similar to the one with low copper ion content.

All low-temperature ESE-detected EPR spectra (Figure S4, Supporting Information) are in agreement with what we have observed already by CW-EPR. The pulsed EPR experiments to detect hyperfine couplings are performed on the hydrogels with 5% $CuCl_2$. The Q-band EPR spectra indicate the typical geometry of an octahedral or distorted octahedral copper complex, as schematically shown in **Figure 7**. All the pulsed EPR measurements were performed on different field positions (shown in **Figure 8**), which reflect different orientations of the copper complex in the g-frame with the most prominent $g_\perp$ and g_{II} positions.

3.3.2. Three Pulse ESEEM Measurements

Three pulse ESEEM data of copper-containing hydrogels 4, 6, 9 (10% $CuCl_2$), and 11 are given in Figure S5 (Supporting Information). They show that the maximum isotropic hyperfine coupling and hence the maximum ^{1}H-nuclear density is localized in the equatorial plane ($g_\perp$ position, *xy*-planar positions, σ_{xy}), which is different from the observation on the axial positions (g_{II}, along *z*-axis, see Figure 7). The decrease of the axial proton hyperfine coupling could be assigned to substitution of these

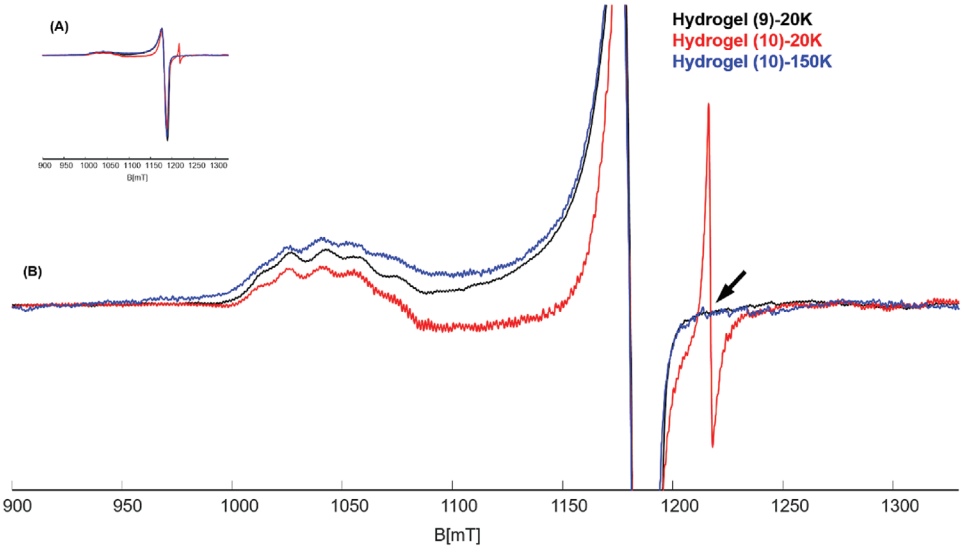

Figure 5. A) EPR spectra of hydrogels with varying calcium/copper salt content. B) The magnified detail plot shows that the sharp signal at B ≈1217 mT (corresponding to g ≈2.001) almost vanishes at 150 K (black arrow) and sharply increases in intensity when cooling down to 20 K. Considering the temperature dependence of the signal, we tentatively assign this to an unknown metal-centered species with different relaxation rates.

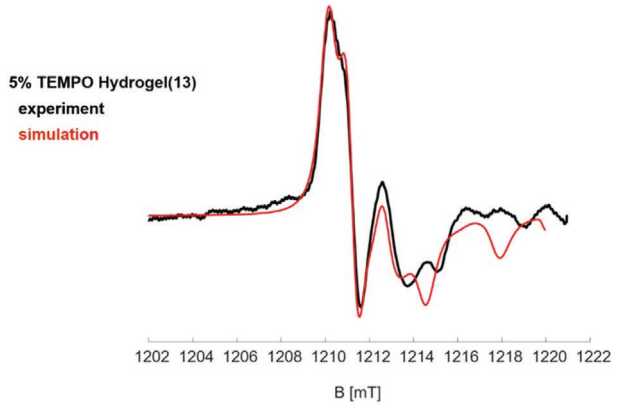

Figure 6. Low temperature (150 K) EPR spectrum of sample 13 (5%TEMPO) (in black) and its simulation (in red). The simulation parameters are given in Table 2.

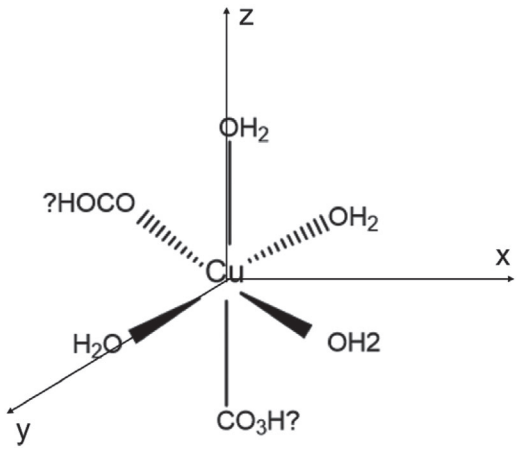

Figure 7. Initial proposed structural model of the copper complex in the composite hydrogel samples based on CW EPR and ESEEM results, depicting the g-tensor principal axis, considering an octahedral coordination shell. Ligands along the *z*-axis are referred as axial ($g_{zz} = g_{II}$) and the ligands located on the *xy* plane are called equatorial ($g_{xy} = g_{\perp}$). To make it clear that at this point carboxylates (HOCO) or carbonates (CO_3H) are only assumed to be bound to the copper center, we have added a question mark to both of them.

positions by ligands other than water, like carbonate anions (which are present in the mixture) and carboxylates (from the polymer chain). Another potential scenario for explaining the ESEEM data is a preferred tetrahedral coordination shell according to Bowron and co-workers.[46] As an initial working model, we propose model 1, based on the CW and ESEEM data (Figure 7).

As we found during sample preparation, it is not possible to form a hydrogel which is cross-linked only by copper ions instead of calcium ions, within the parameters of the here used procedure. Therefore, one may conclude that there is too little direct crosslinking of polymeric chains induced by copper ions to form stable hydrogels but rather viscous solutions ensue. On the molecular level, we found that ligands other than water molecules might occupy the axial positions of the copper complexes in the mixed metal samples (the ligands with question-marks in Figure 7). Therefore, we used ^{13}C-enriched carbonates in ESE-detected and ESEEM experiments (sample 12) to distinguish whether there are couplings between copper and carbonates as ligands as opposed to carboxylates by the polymer. In the three pulse ESEEM measurements, we only observed proton signals. Couplings due to ^{13}C could not be detected, in any of the experiments with different inter-pulse delays (176 or 408 ns) or at any of the field positions.

To better assign the origin of the coupled protons (i.e., if are they solvent- or polymer-related hydrogens), we prepared and measured a solvent mixture of 1:1 of H_2O:^2H_2O (sample 11). Please note that in fully deuterated solvents no hydrogel could be formed.

The ESEEM time traces of samples in pure water (sample 4) and in the semi-deuteriated solvent mixture (sample 11) with their corresponding magnitude spectra at equatorial position are shown in Figure 8. The gyromagnetic ratio of the ^{2}H nucleus is only about 1/6.5 times that of protons. Therefore, at X-band frequencies, remote deuterons appear at a Larmor frequency of ≈2.2 MHz. Sample 11 shows a sharp and intense peak in this frequency region. The ^{2}H peak is a superposition of a narrow peak at 2.2 MHz and a broad peak at around 4 MHz. The sharp

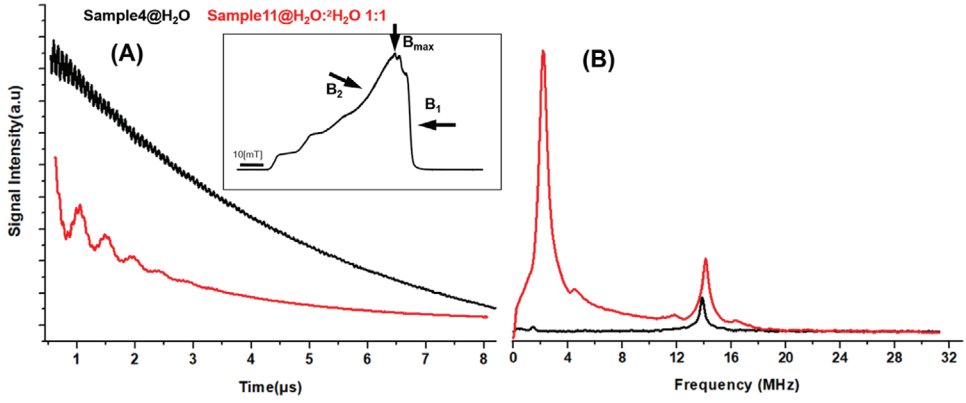

Figure 8. Comparison between ESEEM experiments of two samples 4 and 11 at the equatorial position (B_1) to depict the distribution of solvent molecules around copper center. A) Three pulse ESEEM time traces for a 5% copper containing hydrogel in H_2O (black trace, sample 4) and a solvent mixture H_2O:^2H_2O (red trace, sample 11). The inset shows the examined field positions on the typical ESE of the copper spectrum. B) Corresponding magnitude spectra of the measured samples show a large contribution of ^2H_2O around the copper center.

peak around the Zeeman frequency of deuterium indicates solvent accessibility and $^{1}H/^{2}H$ exchange around the copper cation. The broad peak could be either attributed to the double frequency of ^{2}H nuclei or to the hydrogen-bonded water molecules to the copper center.[47,48] The Larmor frequency of the ^{1}H peak of sample 11, is not only shifted toward higher frequencies (0.3 MHz), but also has an almost double the width, compared to the protonated sample 4 (black trace in **Figure 8**). It also displays two shoulders around ≈11.9 and ≈16.3 MHz which are indicative of combination frequencies between ^{2}H and ^{1}H nuclei. This means that both, hydrogen and deuterium-bearing molecules are simultaneously bound to the same paramagnetic species.

3.3.3. Hyperfine-Sublevel Correlation (HYSCORE) Measurements

To obtain more detailed and resolved information about the hyperfine tensor and local environment around the studied copper complexes, we performed HYSCORE measurements of samples 4, 11, 12, and 8. Moreover, HYSCORE is most valuable to reveal very broad and overlapping signals in ESEEM for their proper assignment.

HYSCORE – Sample 4: The ^{1}H region of the X-band HYSCORE spectra of sample 4 at the equatorial position B_1, shows that the signal is shifted vertically by ≈0.3 MHz from the diagonal line, so that one can initially read out a dipolar coupling of $T \approx 3.9$ MHz (**Figure 9**). Simulations provide an axial hyperfine tensor of $A(^{1}H) = [-2.0, -2.0, 4.0]$ MHz with an Euler angle of $\beta \approx 45°$ between the *g*- and A-tensor frames. Using Equation (3) the $r_{Cu\text{-}H}$ could be obtained as 2.7 Å which is in good agreement with previously reported values for a hexaaqua copper complex.[43,49]

At the axial position, the proton ridge gets smaller, with a vertical shift from diagonal of about 0.37 MHz, producing $T \approx 4.09$ MHz. The principal values of the A-tensor were obtained as [–0.6, –0.6, 1.4] MHz, which is equivalent to $r_{Cu\text{-}H}$ of 2.78 Å. The experimental HYSCORE spectrum and its corresponding simulation, are given in Figure S6 (Supporting Information).

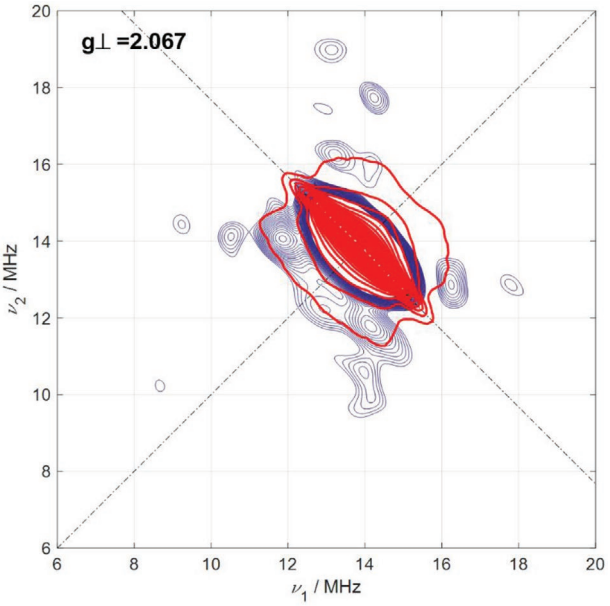

Figure 9. Experimental (marine blue) and simulated (red) ^{1}H-HYSCORE spectra of sample 4 (5% $CuCl_2$) measured at the equatorial field position in the ESE-detected EPR spectrum.

HYSCORE – Sample 11: For sample 11 a vertical shift from the diagonal of ≈0.55 MHz was found at the equatorial position in the ^{1}H nuclear region, yielding a dipolar coupling value of $T \approx 5.00$ MHz (**Figure 10**). Using these data, $r_{C\text{-}H}$ could be estimated as 2.50 Å as described in the experimental section. Further refinement by simulations provided an axial hyperfine tensor $A(^{1}H) = [-0.10, 0.10, 3.00]$ MHz.

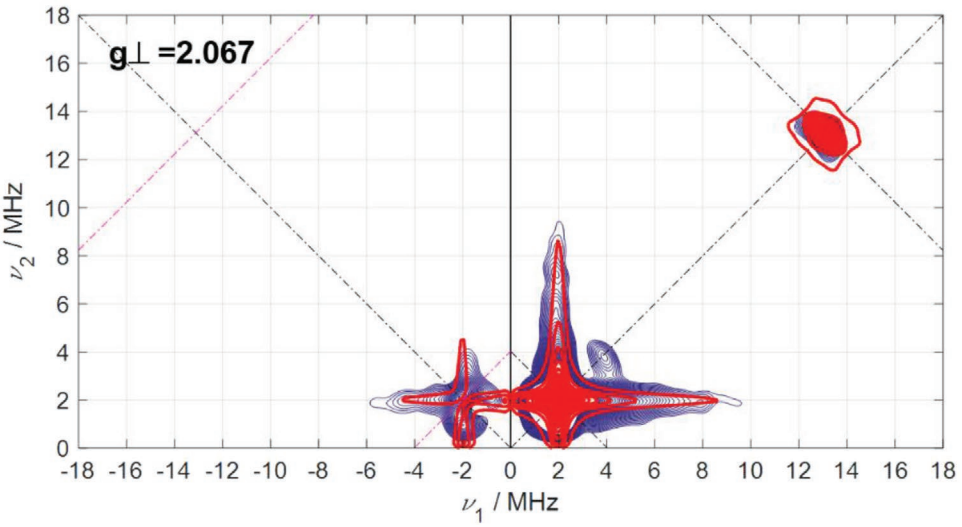

Figure 10. Experimental (marine blue) and simulated (red) ^{1}H-^{2}H HYSCORE spectra of sample 11 containing 5% $CuCl_2$ in a mixed solvent mixture of H_2O:$^{2}H_2O$, 1:1 ratio at $g_\perp = 2.067$. The ^{2}H hyperfine parameters used in the simulations are scaled down by a factor of 6.5 to account for different magneto-gyric ratios of ^{1}H and ^{2}H.

Considering the scale factor of A(^{2}H) = A(^{1}H)/6.5, the ^{2}H region could be simulated with a hyperfine tensor A(^{2}H) = [–0.17, –0.17, 0.24] MHz and a small quadrupole interaction ($|\frac{e^2qQ}{h}|$) of 0.2 MHz and asymmetry parameter $\eta = 0.1$. The dipolar tensor could be estimated as $T_D \approx 2.24$ MHz, corresponding to $r_{Cu\text{-}D} \approx 1.8$ Å using the point-dipole approximation.

These results show contributions from both water isotope molecules at the equatorial plane within the same distance. The experimental and related simulations are given in Figure 10.

Moving toward the axial position, the proton ridge completely disappears. The deuterons show much smaller hyperfine couplings [–0.10, –0.10, 0.30] MHz, while the quadrupolar coupling remains at 0.25 MHz. However the asymmetry parameter gets smaller $\eta = 0.05$, indicating a more isotropic pattern. The dipolar coupling could be estimated as $T_D \approx 2.0$ MHz, which returns $r_{Cu\text{-}D} \approx 1.8$ Å. The experimental spectra and their simulations are shown in Figure S7 (Supporting Information) (**Table 3**).

HYSCORE-Samples 8 and 12: In this part, we investigate if there are any carbon nuclear spins coupled to the copper center, either from polymer-based carboxylates (sample 8, NaOH instead of carbonates) or from carbonates (sample 12, ^{13}C-labeled carbonates).

Measuring HYSCORE at the equatorial position in the ESE-detected EPR spectrum of sample 8, one finds that the proton ridge has a vertical shift of ≈0.30 MHz, producing T = 3.83 MHz, returning the known value of $r_{Cu\text{-}H} = 2.70$ Å. Simulations gave A(^{1}H) = [–1.00, –1.00, 3.20] MHz, with an A_{iso} = 0.40 MHz.

At the axial position, a short proton ridge with an almost purely dipolar contribution could be reproduced by an axial hyperfine tensor [–0.10, –0.10, 1.00] MHz. The dipolar contribution is thus found as 2.30 MHz, observing the vertical shift (0.12 MHz) from the diagonal. The copper hydrogen bond length is thus about 3.40 Å using the point-dipole approximation. Experimental and simulated spectra at different field positions are given in Figure S8 (Supporting Information).

We could not detect any evidence of (even remote) couplings between carbons and the copper center. When taking into account the observation that no hydrogels form when only copper salts are used, this is circumstantial evidence that there are no or only little copper-bound carboxylates in sample 8.

Sample 12, prepared with isotope-labeled $Na_2{}^{13}CO_3$ did not show any signal at the Larmor frequency of carbon-13 nuclei. Therefore, the possibility of carbonates directly ligated to the copper cation is also unlikely. Looking at the proton region of the spectra, we found similar results as in sample 4 for equatorial protons (B_1) with $r_{Cu\text{-}H} = 2.70$ Å.

The HYSCORE spectra recorded at the axial positions indicate two kinds of protons: one of a small of hyperfine tensor [–0.60, –0.60, 1.40] MHz, which could stem from contributions of protons that are intermediate in position and span from the equatorial to the axial region. The second type of protons has an A(^{1}H) = [–1.00, –1.00, 4.50] MHz and a dipolar contribution of ≈3.36 MHz. These are axial protons with a $r_{Cu\text{-}H} = 3.0$ Å. Corresponding HYSCORE spectra with their simulation are given in Figure S9 (Supporting Information).

3.4. Proposed Structure of Copper Complexes and their Position in the Hydrogel Network

HYSCORE of sample 4 at the equatorial position reveals a Cu-H distance of 2.70 Å which is in good agreement with the distance obtained already by Atherton et al. for a $[Cu(H_2O)_6]^{2+}$ complex.[43] Using structural data of the copper hexaaqua complex ($r_{Cu\text{-}O}$ = 2.2 Å, $r_{O\text{-}H}$ = 1.0 Å, <Cu-O-H = 109°, considering a sp^3 hybridization), we could estimate a Cu-O bond length as 2.0 Å, which is in correspondence with equatorial water molecules. The distance of 2.8 Å at the axial position, however, may indicate a compression of axial bonds for this complex, assuming a copper ion with six ligands in its coordination shell. Another possible explanation is the complete removal of direct ligands at the axial position(s) and formation of a copper complex with lower coordination number, e.g., with a square pyramidal geometry of a $[Cu(H_2O)_5]^{2+}$ complex as found by MD simulations by Almeida and coworkers.[50] These authors also found that by decreasing coordination number, the average bond lengths of Cu-O and Cu-H decrease, as well. We observed similar results here for sample 11.

The scenario is different for sample 8 and 12 and there is a distinct difference between axial and equatorial bond lengths. Sample 8 yields Cu-H distances of 2.7 and 3.4 Å at equatorial and axial positions, respectively. These bond lengths are in good agreement with a hexaaqua copper complex. Considering the structural information of this complex, an axial distance of 2.6 Å could be estimated for Cu-O bond length, which shows this bond is elongated by 0.4 Å, compared to a(n) isolated hexaaqua copper complex. In case of sample 12, the axial and equatorial protons could be well distinguished from each other as well. The obtained distances from HYSCORE are in good agreement with a hexaaqua copper complex, too.

Taken together, we find that in most samples, minute isotropic hyperfine couplings pertain along both, axial and equatorial positions. This indicates that all these protons are involved in hydrogen bonds outside the copper complexes.[51–54] It also shows that copper cations increase their coordination number by addition of water molecules to their first solvation shell, which is energetically favorable.[55] Formation of molecular clusters by increased hydrogen bonding is then reflected

Table 3. Experimental hyperfine couplings (in MHz) and distances $r_{Cu\text{-}X}$ (X = H, D in Å) for sample 11.

Sample	Nucleus	I	[A]	$[\alpha, \beta, \gamma]^A$	$[Q, \eta]$	$[\alpha, \beta, \gamma]^Q$	A_{iso}	T	R (Cu-X)
$g_\perp = 2.067$									
11	H	1/2	–1.10, –1.10, 1.60	5, 65, 5	–	–	–0.20	4.90	2.50
	D	1	–0.17,–0.17, 0.24	–	0.20, 0.10	5, 40, 5	–0.03	2.24	1.74
$g_{II} = 2.352$									
11	D	1	–0.10, –0.10, 0.30		0.25, 0.05	5, 30, 5	0.03	2.07	1.87

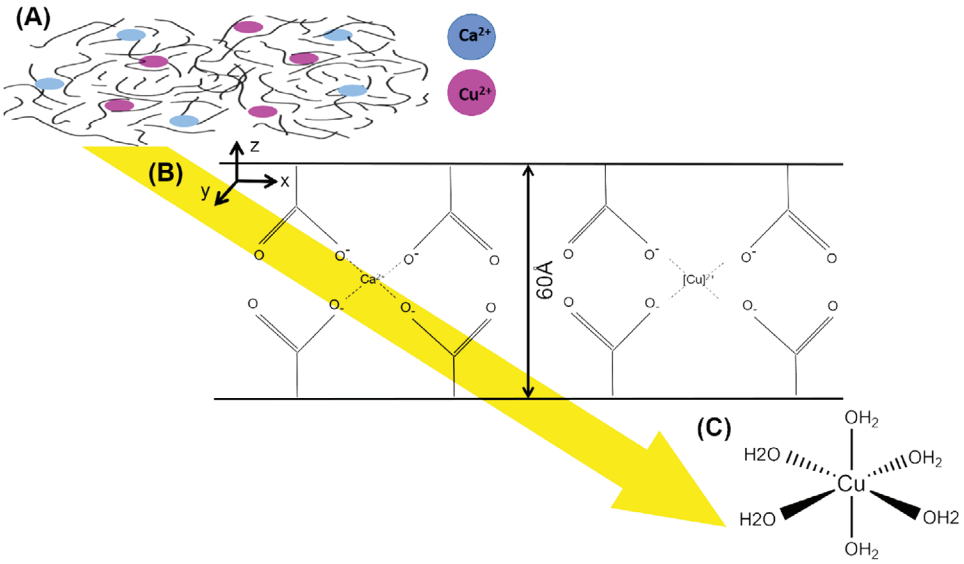

Figure 11. Macroscopic (top) to microscopic (bottom) view as shown by the yellow arrow. A) The hydrogel contains calcium and copper cations in planar view. B) In such schematic layer, calcium cations are covalently bound to the carboxylate groups, while copper cations make different complexes and locate in the hollow spaces between layers. C) Suggested copper complex is hydrogen bonded to the PAA layers.

macroscopically, especially in the highly adhesive property of hydrogels prepared with sodium hydroxide (samples 3 and 8).

4. Conclusions

Considering all these observations, we conclude that in copper salt-containing hydrogels, copper cations are found and remain in their hexaaqua (or distorted, e.g., as a pseudo "tetra-aqua") complex state and only as these rather large complex cations interact with the anions of PAA through electrostatic interactions. The charge densities of the water-based copper complexes are of course much lower than for the corresponding naked copper or calcium cations. In contrast, in the conventional reference hydrogel (sample 1) calcium ions may prefer direct, close electrostatic interactions with the carboxylic anions of the side chains of polymer. Addition of this charge-screened second interaction mediated through copper ions can explain the improved elastic properties of copper containing hydrogels. A pictorial summary of this molecular interpretation is given in **Figure 11**. The height of an end-tethered PAA layer at pH ≈8 and a calcium ion concentration $\approx 0.1 \times 10^{-3}$ M has been estimated as ≈6.0 nm in a theoretical study.[56] In addition, the anion effect (sulfate vs chloride) of the copper salts on the mechanical properties can be explained in a straightforward fashion: due to the larger anionic charge, the sulfates may still cluster close to divalent cations (copper and probably also calcium) and either prevent copper inclusion in the polymer-carboxylate-rich regions altogether or screen/shield their cationic charge more effectively. This is not the case in copper chloride based hydrogels, which thus have even stronger mechanical properties. The use of D_2O as a solvent and the subsequent change its use brings for the H-bonding abilities[57] of the polymer, the copper hexaaqua complex and the calcium ions, sheds light on the role of H-bonding networks during and after gel formation. The hydrated copper complexes may well stabilize hydrogen-bonded water networks in the water-filled polymer regions.

The use of hydrated copper ions may thus be seen as simple means to increase the elastic properties through dampened electrostatic interactions on the one hand and the viscous properties through maintaining the larger hydrogen-bonded water networks in the polymer hydrogels. Either of these features, in return, may be desirable for certain applications. Moreover, the use of trivalent hydrated metal complexes might be interesting to further fine-tune the elastic and viscous properties of these simple yet remarkably robust hydrogels. In particular when exploring possibilities to implement magnetic properties inside water based gels, this might be of great interest.

Supporting Information

Supporting Information is available from the Wiley Online Library or from the author.

Acknowledgements

The authors thank Annekatrin Rother and Heike Schimm (both MLU) for technical support. This research was financially supported by financial support from the state of Saxony-Anhalt (European Regional Development Fund–ERDF grant ZS/2016/06/79740).

Open access funding enabled and organized by Projekt DEAL.

Conflict of Interest

The authors declare no conflict of interest.

Keywords

composite materials, EPR, HYSCORE, metal containing hydrogels, mineral plastics, polymeric hydrogels

Received: August 11, 2020
Revised: September 25, 2020
Published online: November 12, 2020

[1] G. Sadowski, W. Richtering, *Intelligent Hydrogels: Progress in Colloid and Polymer Science*, Vol. 140 (Eds: F. Kremer, W. Richtering), Springer, Germany **2013**.
[2] O. Wichterle, D. Lim, *Nature* **1960**, *185*, 117.
[3] M. Bahram, N. Mohseni, M. Moghtader, *Introduction to Hydrogel and Some Recent Applications*, IntechOpen, London **2016**.
[4] M. V. Ghica, M. Hîrjau, D. Lupuleasa, C. E. Dinu-Pîrvu, *Molecules* **2016**, *21*, 786.
[5] Y. Shi, L. Peng, Y. Ding, Y. Zhao, G. Yu, *Chem. Soc. Rev.* **2015**, *44*, 6684.
[6] M. S. Rahman, M. M. Islam, M. S. Islam, A. Zaman, T. Ahmed, S. Biswas, S. Sharmeen, T. U. Rashid, M. M. Rahman, *Polymers and Polymeric Composites: A Reference Series* (Ed: Md. I. H. Mondal), Springer International Publishing AG, part of Springer Nature, Cham, Switzerland **2018**.
[7] D. Lee, H. Zhang, S. Ryu, in *Cellulose-Based Superabsorbent Hydrogels, Polymers and Polymeric Composites: A Reference Series* (Ed: Md. I. H. Mondal), Springer International Publish. AG, part of Springer Nature, Cham, Switzerland **2018**.
[8] L. L. E. Mears, E. R. Draper, A. M. Castilla, H. Su, B. D. Zhuola, M. C. Nolan, G. N. Smith, J. Doutch, S. Rogers, R. Akhtar, H. Cui, D. J. Adams, *Biomacromolecules* **2017**, *18*, 3531.
[9] H. Li, P. Yang, P. Pageni, C. Tang, *Macromol. Rapid Commun.* **2017**, *38*, 1700109.
[10] S. Sun, L. B. Mao, Z. Lei, S. H. Yu, H. Cölfen, *Angew. Chem., Int. Ed. Engl.* **2016**, *55*, 11765.
[11] D. J. Schupp, X. Zhang, S. Sun, H. Cölfen, *Chem. Commun.* **2019**, *55*, 4913.
[12] K. Mikula, D. Skrzypczak, B. Ligas, A. Witek-Krowiak, *SN Appl. Sci.* **2019**, *1*, 643.
[13] J. Nie, Z. Wang, Q. Hu, *Sci. Rep.* **2016**, *6*, 36005.
[14] A. Kaufman Katz, J. P. Glusker, S. A. Beebe, C. W. Bock, *J. Am. Chem. Soc.* **1996**, *118*, 5752.
[15] A. Schweiger, G. Jeschke, *Principles of Pulse Electron Paramagnetic Resonance*, Oxford University Press, Oxford **2001**.
[16] D. Hinderberger, *Topics in Current Chemistry*, Vol. 321 (Eds: M. Drescher, G. Jeschke), Springer-Verlag, Berlin Heidelberg, Germany **2012**.
[17] I. Krstic, A. Marko, C. M. Grytz, B. Endeward, T. F. Prisner, in *RNA Structure and Folding, Biophysical Techniques and Prediction Methods* (Eds: Hrsg. V. Klostermeier, D. Hammann, Ch. De Gruyter), Walter de Grutyer, Berlin **2013**, pp. 261–286.
[18] M. J. N. Junk, U. Jonas, D. Hinderberger, *Small* **2008**, *4*, 1485.
[19] S. H. Arabi, B. Aghelnejad, C. Schwieger, A. Meister, A. Kerth, D. Hinderberger, *Biomater. Sci.* **2018**, *6*, 478.
[20] D. Kurzbach, M. J. N. Junk, D. Hinderberger, *Macromol. Rapid Commun.* **2013**, *34*, 119.
[21] J. Hunold, T. Wolf, F. R. Wurm, D. Hinderberger, *Chem. Commun.* **2019**, *55*, 3414.
[22] H. H. Haeri, J. Blaffert, F. A. Schöffmann, M. Blech, J. Hartl, P. Garidel, D. Hinderberger, *Molecules* **2019**, *24*, 2528.
[23] E. L. Hahn, *Phys. Rev.* **1950**, *80*, 580.
[24] L. G. Rowan, E. L. Hahn, W. B. Mims, *Phys. Rev. A* **1965**, *137*, B1491.
[25] J. M. Fauth, A. Schweiger, L. Braunschweiler, J. Forrer, R. R. Ernst, *J. Magn. Reson.* **1969**, *66*, 74.
[26] A. Volkov, C. Dockter, T. Bund, H. Paulsen, G. Jeschke, *Biophys. J.* **2009**, *96*, 1124.
[27] L. Bottorf, I. D. Sahu, R. M. McCarrick, G. A. Lorigan, *Biochim. Biophys. Acta, Biomembr.* **2018**, *1860*, 1447.
[28] P. Höfer, A. Grupp, G. Nebenführ, M. Mehring, *Chem. Phys. Lett.* **1986**, *132*, 279.
[29] A. Pöppl, L. Kevan, *J. Phys. Chem.* **1996**, *100*, 3387.
[30] S. Van Doorslaer, E. Vinck, *Phys. Chem. Chem. Phys.* **2007**, *9*, 4620.
[31] J. A. Weil, J. R. Bolton, *Electron Paramagnetic Resonance: Elementary Theory and Practical Applications*, 2nd ed., John Wiley & Sons, Inc, New Jersey **2007**.
[32] S. Stoll, A. Schweiger, *J. Magn. Reson.* **2006**, *178*, 42.
[33] L. Bromberg, M. Temchenko, V. Alakhov, T. A. Hatton, *Int. J. Pharm.* **2004**, *282*, 45.
[34] N. Hall, M. Orio, M. Gennari, C. Wills, F. Molton, C. Philouze, G. B. Jameson, M. A. Halcrow, A. G. Blackman, a. C. Duboc, *Inorg. Chem.* **2016**, *55*, 1497.
[35] E. Garribba, G. Micera, *J. Chem. Educ.* **2006**, *83*, 1229.
[36] N. K. Solanki, E. J. L. McInnes, F. E. Mabbs, S. Radojevic, M. McPartlin, N. Feeder, J. E. Davies, M. A. Halcrow, *Angew. Chem., Int. Ed.* **1998**, *37*, 2221.
[37] B. J. Hathaway, *J. Chem. Soc., Dalton Trans.* **1972**, 1196.
[38] B. J. Hathaway, D. E. Billing, *Coord. Chem. Rev.* **1970**, *5*, 143.
[39] R. D. Shannon, *Acta Crystallogr.* **1976**, *32*, 751.
[40] H. D. B. Jenkins, K. P. Thakur, *J. Chem. Educ.* **1979**, *56*, 576.
[41] A. Godiksen, F. N. Stappen, P. N. R. Vennestrøm, F. Giordanino, S. B. Rasmussen, L. F. Lundegaard, S. Mossin, *J. Phys. Chem. C* **2014**, *118*, 23126.
[42] F. Giordanino, P. N. Vennestrøm, L. F. Lundegaard, F. N. Stappen, S. Mossin, P. Beato, S. Bordiga, C. Lamberti, *Dalton Trans.* **2013**, *42*, 12741.
[43] P. M. Schosseler, B. Wehrli, A. Schweiger, *Inorg. Chem.* **1997**, *36*, 4490.
[44] J. Hunold, J. Eisermann, M. Brehm, D. Hinderberger, *J. Phys. Chem. B* **2020**, *124*, 8601.
[45] P. J. Carl, D. E. W. Vaughan, D. Goldfarb, *J. Phys. Chem. B* **2002**, *106*, 5428.
[46] D. T. Bowron, M. Amboage, R. Boada, A. Freeman, S. Hayama, S. D. Moreno, *RSC Adv.* **2013**, *3*, 17803.
[47] R. Carmieli, N. Papo, H. Zimmermann, A. Potapov, Y. Shai, D. Goldfarb, *Biophys. J.* **2006**, *90*, 492.
[48] D. A. Erilov, R. Bartucci, R. Guzzi, A. A. Shubin, A. G. Maryasov, D. Marsh, S. A. Dzuba, L. Sportelli, *J. Phys. Chem. B* **2005**, *109*, 12003.
[49] N. M. Atherton, A. J. Horsewill, *Mol. Phys.* **1979**, *37*, 1349.
[50] K. J. Almeida, N. A. Murugan, Z. Rinkevicius, H. W. Hugosson, O. Vahtras, H. Agren, A. Cesar, *Phys. Chem. Chem. Phys.* **2009**, *11*, 508.
[51] P. J. O'Mally, G. T. Babcock, *J. Am. Chem. Soc.* **1986**, *108*, 3995.
[52] S. Grimaldi, R. A. Cartin, P. Lanciano, S. Lyubenova, R. Szenes, B. Endeward, T. F. Prisner, B. Guigliarelli, A. Magalon, *J. Biol. Chem.* **2012**, *287*, 4662.
[53] F. MacMillan, F. Lendzian, W. Lubitz, *Magn. Reson. Chem.* **1995**, *33*, S81.
[54] M. Flores, R. A. Isaacson, R. Calvo, G. Feher, W. Lubitz, *Chem. Phys.* **2003**, *294*, 401.
[55] V. S. Bryantsev, M. S. Diallo, A. C. T. van Duin, W. A. GoddardIII, *J. Phys. Chem. A* **2008**, *112*, 9104.
[56] R. J. Nap, I. Szleifer, *J. Chem. Phys.* **2018**, *149*, 163309.
[57] A. K. Soper, C. J. Benmore, *Phys. Rev. Lett.* **2008**, *101*, 065502.